clones overexpressing pathogenic α-synuclein mutants exhibited slower rates of long-lived protein degradation, and the remaining lysosomal protein degradation was completely blocked by 3-methyladenine, consistent with a blockade of CMA and compensatory activation of macroautophagy. These results could explain the degradation by macroautophagy of mutant, but not wild-type, α-synuclein proteins (*13*) (supporting online text 2). The induction of macroautophagy following blockade of normal CMA by mutant α-synucleins appears consistent with observations in cultured fibroblasts, in which blockade of CMA leads to compensatory activation of macroautophagy (*28*), as well as with the induction of neuronal macroautophagy by a number of stress paradigms, including the overexpression of the mutant α-synucleins (*16*, *29*).

Thus, wild-type α-synuclein is efficiently degraded in lysosomes by CMA, but the pathogenic α-synuclein mutations are poorly degraded by CMA despite a high affinity for the CMA receptor. Mutant α-synucleins blocked the lysosomal uptake and degradation of other CMA substrates. CMA blockade then results in a compensatory activation of macroautophagy which, under these conditions, cannot maintain normal rates of protein degradation. Impaired CMA of pathogenic α-synuclein may favor toxic gains-of-functions by contributing to its aggregation or additional modifications, such as nitrated or dopamine-adduct formation that could further underlie PD and other synucleinopathies (*3*). Mutant α-synuclein also inhibits the degradation of other long-lived cytosolic proteins by CMA, which may further contribute to cellular stress, perhaps causing the cell to rely on alternate degradation pathways or to aggregate damaged proteins.

References and Notes

1. A. Abeliovich *et al.*, *Neuron* **25**, 239 (2000).
2. R. L. Nussbaum, M. H. Polymeropoulos, *Hum. Mol. Genet.* **6**, 1687 (1997).
3. W. Dauer, S. Przedborski, *Neuron* **39**, 889 (2003).
4. M. C. Bennett *et al.*, *J. Biol. Chem.* **274**, 33855 (1999).
5. G. K. Tofaris, R. Layfield, M. G. Spillantini, *FEBS Lett.* **509**, 22 (2001).
6. K. S. McNaught, C. W. Olanow, O. Halliwell, O. Isacson, P. Jenner, *Nat. Rev. Neurosci.* **2**, 589 (2001).
7. K. Ancolio, C. Alves da Costa, K. Ueda, F. Checler, *Neurosci. Lett.* **285**, 79 (2000).
8. H. J. Rideout, K. E. Larsen, D. Sulzer, L. Stefanis, *J. Neurochem.* **78**, 899 (2001).
9. H. J. Rideout, L. Stefanis, *Mol. Cell. Neurosci.* **21**, 223 (2002).
10. M. H. Glickman, A. Ciechanover, *Physiol. Rev.* **82**, 373 (2002).
11. J. F. Dice, *Lysosomal Pathways of Protein Degradation* (Landes Bioscience, Austin, TX, 2000).
12. A. M. Cuervo, *Trends Cell Biol.* **14**, 70 (2004).
13. J. Webb, B. Ravikumar, J. Atkins, J. Skepper, D. Rubinsztein, *J. Biol. Chem.* **278**, 25009 (2003).
14. E. Paxinou *et al.*, *J. Neurosci.* **21**, 8053 (2001).
15. H. Lee, F. Khoshaghideh, S. Patel, S. J. Lee, *J. Neurosci.* **24**, 1888 (2004).
16. L. Stefanis, K. E. Larsen, H. J. Rideout, D. Sulzer, L. A. Greene, *J. Neurosci.* **21**, 9549 (2001).
17. C. Wilson *et al.*, *J. Cell Biol.* **165**, 335 (2004).
18. A. M. Cuervo, J. F. Dice, *J. Mol. Med.* **76**, 6 (1998).
19. A. M. Cuervo, J. F. Dice, *Science* **273**, 501 (1996).
20. A. M. Cuervo, J. F. Dice, E. Knecht, *J. Biol. Chem.* **272**, 5606 (1997).
21. J. F. Dice, *Trends Biochem. Sci.* **15**, 305 (1990).
22. Materials and methods are available as supporting material on *Science* Online.
23. A. M. Cuervo, S. R. Terlecky, J. F. Dice, E. Knecht, *J. Biol. Chem.* **269**, 26374 (1994).
24. N. Salvador, C. Aguado, M. Horst, E. Knecht, *J. Biol. Chem.* **275**, 27447 (2000).
25. M. J. Volles *et al.*, *Biochemistry* **40**, 7812 (2001).
26. V. Grantcharova, E. Alm, D. Baker, A. Horwich, *Curr. Opin. Struct. Biol.* **11**, 70 (2001).
27. G. Fuertes, J. J. Martin De Llano, A. Villaroya, A. J. Rivett, E. Knecht, *Biochem. J.* **375**, 75 (2003).
28. A. C. Massey, G. Sovak, A. M. Cuervo, unpublished results.
29. K. Larsen, D. Sulzer, *Histol. Histopathol.* **17**, 897 (2002).

30. We are very grateful to B. Giasson and V. Lee for providing us with a human-specific monoclonal antibody to α-synuclein (Syn 211) and to Q. Wang and A. Massey for technical assistance. This work was supported by the NIH/National Institute on Aging grant AG021904 (A.M.C.), two National Institute of Neurological Disorders and Stroke Udall Center grants (D.S. and P.L.), the Parkinson's Disease Foundation, the Lowenstein Foundation (L.S. and D.S.), the Matheson Foundation (L.S.), a Huntington's Disease Society of America Grant (D.S. and A.M.C.), and the Howard Hughes Medical Institute (A.M.C.). Molecular interaction data have been deposited in the Biomolecular Interaction Network Database with accession code 151734.

Supporting Online Material

www.sciencemag.org/cgi/content/full/305/5688/1292/DC1
Materials and Methods
SOM Text
Figs. S1 to S4
References

21 June 2004; accepted 23 July 2004

Distinct Ensemble Codes in Hippocampal Areas CA3 and CA1

Stefan Leutgeb,[1] Jill K. Leutgeb,[1] Alessandro Treves,[1,2] May-Britt Moser,[1] Edvard I. Moser[1]*

The hippocampus has differentiated into an extensively connected recurrent stage (CA3) followed by a feed-forward stage (CA1). We examined the function of this structural differentiation by determining how cell ensembles in rat CA3 and CA1 generate representations of rooms with common spatial elements. In CA3, distinct subsets of pyramidal cells were activated in each room, regardless of the similarity of the testing enclosure. In CA1, the activated populations overlapped, and the overlap increased in similar enclosures. After exposure to a novel room, ensemble activity developed slower in CA3 than CA1, suggesting that the representations emerged independently.

The hippocampus plays a fundamental role in encoding, consolidation, and retrieval of episodic and semantic memory (*1–4*). In mammals, the hippocampus has differentiated into a recurrent network of densely interconnected pyramidal cells (CA3) and a feed-forward network with almost no intrinsic excitatory connections (CA1) (*5*). These structural differences suggest distinct roles for CA3 and CA1 in hippocampal memory formation, but which functions are performed by the two subfields has remained elusive (*6*).

Firing properties of individual pyramidal cells in CA3 and CA1 offer limited clues about computational advantages of hippocampal differentiation. In both subfields, the majority of pyramidal cells have place-specific firing fields controlled by geometric relations in the animal's local environment (*2*, *7–10*), and there are only small quantitative differences in their spatial firing characteristics (*10*). However, cell assemblies in CA3 and CA1 may contain additional information (*11*). A major function of such assemblies may be to augment differences between correlated input patterns (*1*, *8*, *12–18*) so as to minimize interference between stored information (*19*). To examine whether such an orthogonalization process (pattern separation) (*20*) is implemented differentially in CA3 and CA1, we compared ensemble firing in connected segments of these areas (*5*) (Fig. 1A) while rats were chasing food in enclosures with varying geometric similarity (large square, small square, and small circle) in three different rooms (A, B, and C).

Individual place cells in CA3 and CA1 had similar firing characteristics (*7*, *10*, *21*) (Fig. 2A and tables S1 and S2). The most obvious difference was the significantly lower proportion of active neurons in CA3 (*10*). With a rate threshold of 0.25 Hz, the

[1]Centre for the Biology of Memory, Medical-Technical Research Centre, Norwegian University of Science and Technology, 7489 Trondheim, Norway. [2]Cognitive Neuroscience Sector, International School for Advanced Studies, Trieste, Italy.

*To whom correspondence should be addressed. E-mail: edvard.moser@cbm.ntnu.no

proportion of active cells ranged from 0.17 (B) to 0.32 (A) in CA3 and from 0.48 (C) to 0.66 (A) in CA1 (z values from 4.1 in C to 8.0 in A, $P < 0.001$) (Fig. 1, B to D, and fig. S1). The sparser firing of CA3 may indeed favor more orthogonal representations, but it cannot be established from discharge profiles in a single condition whether active orthogonalization takes place. To examine orthogonalization processes more directly, we quantified the extent to which the active set of neurons overlapped between two familiar rooms (A and B) by using a measure that takes into account the passive effect of different sparsity in CA3 and CA1 (Fig. 2B).

The analyses indicated that ensemble codes in CA3 and CA1 are different (Fig. 2B). In CA3, representations for A and B were nearly independent. The measured overlap ranged from 0.11 to 0.14 for the four possible comparisons of A and B (AB, AB′, A′B, and A′B′, where A and B are the first 10-min blocks in each room and A′ and B′ the second). These values were not significantly different from the expected overlap for independent firing, which ranged from 0.12 to 0.14 depending on exact firing rate distributions between A, B, B′, and A′ (Fig. 2B) (t values between 0.1 and 1.2). The distribution of CA3 population vectors was highly informative about which room the rat was in [0.54 ± 0.06 bits at time bin (τ) = 150 ms, mean ± SEM]. In CA1, however, there was significant overlap between the representations for A and B. Observed values ranged from 0.36 to 0.42, whereas expected values were between 0.26 and 0.28 (t values between 3.7 and 5.2, all $P < 0.001$). Population vectors differed less than in CA3 [0.30 ± 0.05 bits for CA1 at τ = 150; $t(17) = 3.2$, $P < 0.005$].

We hypothesized that the correlated activity in CA1 depended on the distinctness of A and B and thus compared the overlap obtained with similar and different enclosures in these rooms (Fig. 2C and figs. S2 and S3). Shared features had no effect in CA3 (Fig. 2C). With identical square boxes in A and B (high similarity), the overlap in CA1 was almost as large as with repeated testing in the same room (0.55 for AB versus 0.63 for AA′ and 0.66 for BB′). With squares of different size (medium similarity), the overlap decreased to 0.43. With boxes that differed both in size and shape (low similarity), the overlap was no longer distinguishable from the expected value obtained with random permutations (0.32 versus 0.28). These effects were statistically significant [$F(2,140) = 6.0$, $P < 0.005$] and consistent across animals (high similarity values were 0.56 and 0.54; medium similarity, 0.53, 0.45, and 0.32; low similarity, 0.41, 0.34, and 0.27). These effects were also seen in spatial correlations between pairs of firing fields in A and B (Fig. 2D) and in the temporal structure of the ensemble activity (Fig. 2E) [Supporting Online Material (SOM) Text].

Place fields develop as animals explore novel environments (*2*, *9*). We asked whether differences between CA3 and CA1 emerge gradually or are present from the beginning in rats exposed to a novel room (room C) (Fig. 3). In CA3, the overlap between C and A or B fluctuated around expected values (0.16 versus 0.14) [$t(83) = 0.79$, NS], implying that new representations were decorrelated already on the first trial (Fig. 3B). In CA1, the new representations correlated significantly with those in A and B [overlap of 0.38; expected value of 0.24; $t(104) = 4.6$, $P < 0.001$]. This overlap in CA1 was not influenced by the geometry of the enclosures (Fig. 3B) [$t(63) = 0.0$ for medium versus low similarity].

To determine whether the ensemble codes in CA1 derive from those in CA3, we next compared their time courses. In CA3, the new spatial map stabilized only after 20 to 30 min in C (Fig. 3A). The overlap between the first and the last 10-min blocks (CC′′) was low compared to the overlap between repeated trials in the familiar rooms (AA′ and BB′) (Fig. 3C versus Fig. 2B). The distribution of population vectors was more different between the first and the last 10 min (CC′′) than between the first and the middle 10 min (CC′) (Fig. 3, D and E) (SOM Text), suggesting that the stabilization of the ensemble structure in CA3 took 20 min or more. In simultaneously recorded CA1 cells, reliable place fields were mostly apparent already during the first minutes (*9*). The overlap between the first and last 10 min was higher than that for CA3 [$t(91) = 5.1$, $P < 0.001$] (Fig. 3C), and the population-vector distributions were more similar (Fig. 3, D and E) and not significantly different from those obtained between repeated tests in A or B (SOM Text). The faster manifestation of an ensemble code in CA1 suggests that representations in CA3 and CA1 arise independently and that the latter may emerge through direct input from the entorhinal cortex (*22*).

The functional differences between CA3 and CA1 suggest a rationale for the differentiation of their intrinsic structure (*6*).

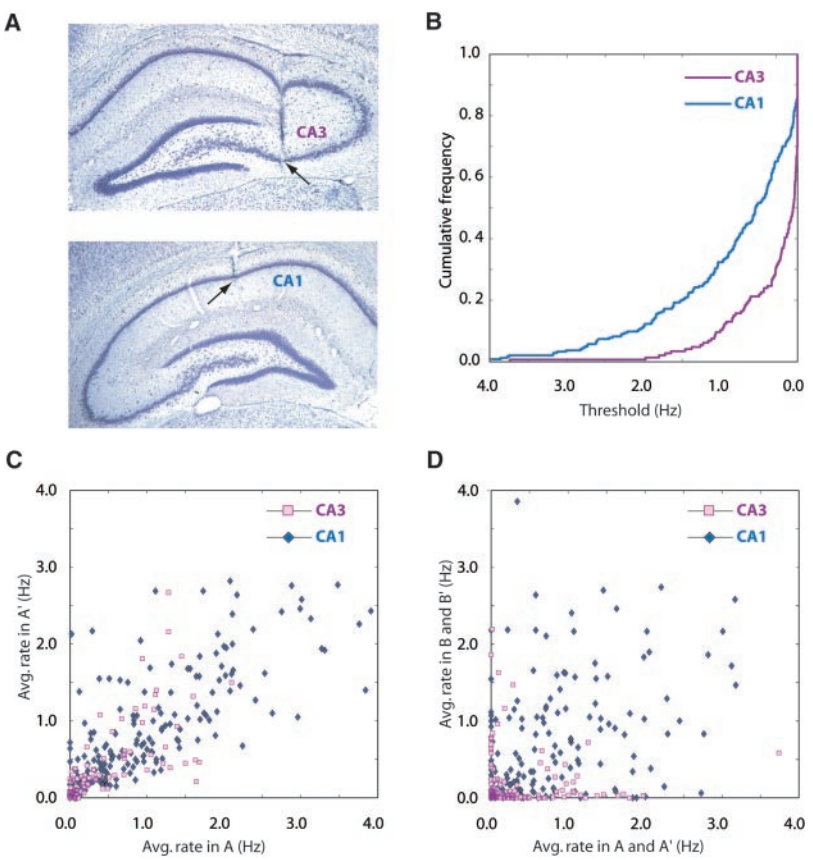

Fig. 1. Sparser representations in CA3 than CA1. (**A**) Representative electrode locations (arrows) in CA3 and CA1 (same rat). (**B**) Cumulative frequency diagram showing lower proportion of active cells in CA3 than CA1 in room A (all cells; see also fig. S1). (C and D) Relation between firing rates on repeated tests in the same room (**C**) or in different rooms (**D**). Each point corresponds to one cell.

With its orthogonalized activity patterns, CA3 may store accurate representations of context one in one, with the representation of local position by individual neurons. This provides a neuronal substrate for the observation that animals with hippocampal lesions show increased susceptibility to interference (*19*) and fail to discriminate between contexts with different conditioning histories, particularly when the contexts differ only minimally (*23*, *24*). As input similarity increases, the CA3 network may eventually switch from pattern separation to pattern completion (*1*, *12*, *25*, *26*), resulting in a larger overlap in CA3 than in CA1 (*26*) and suggesting that CA3 contains coherent but flexible population codes that can be used both to disambiguate and to identify contexts (*27*). Taken together, the findings imply that encoding of context, defined as the relations between stimuli and the time and place in which events occur, may be a major function of CA3 (*2*–*4*, *28*, *29*). Although pattern separation and pattern completion probably arise within the dentate/CA3 complex (*13*, *15*), the exact contribution of the dentate to ensemble activity in CA3 remains to be elucidated.

In contrast to CA3, population codes in CA1 responded to common features of the rooms. When rats were tested with identical boxes in two different rooms, representations in CA1 were only weakly more different than during repeated recording in the same room. This suggests that place cells in CA1 can respond to individual landmark configurations independently of background context, as observed after cue misalignments in CA1 (*26*, *30*, *31*) (SOM Text). However, orthogonalized codes from CA3 may be reflected in equally orthogonal representations in CA1 under certain conditions, such as with low sensory input and during memory-based behavior. The orthogonalized codes may then be exported to other brain structures (*32*, *33*), associating a contextual tag to information stored there.

New representations formed at a slower rate in CA3 than in CA1. The slower manifestation of a stable map in CA3 may, perhaps, reflect the predominantly recurrent nature of interactions in this network, which may require that a stable orthogonalized representation of a new context be reached iteratively. In contrast, the population activity in the predominantly feedforward network of CA1 may be established at the very beginning of the trial or even be available beforehand, hardwired in the circuit (*27*). The faster appearance of the CA1 ensemble code suggests that it emerges independently of the CA3 representation, probably via the direct projections from entorhinal cortex (*22*). However, representations in CA1 may still evolve further. The relation between geometric similarity and overlap was not expressed on day 1 in the novel room, suggesting that the more limited disambiguation of differences in CA1 is a later refinement, like other

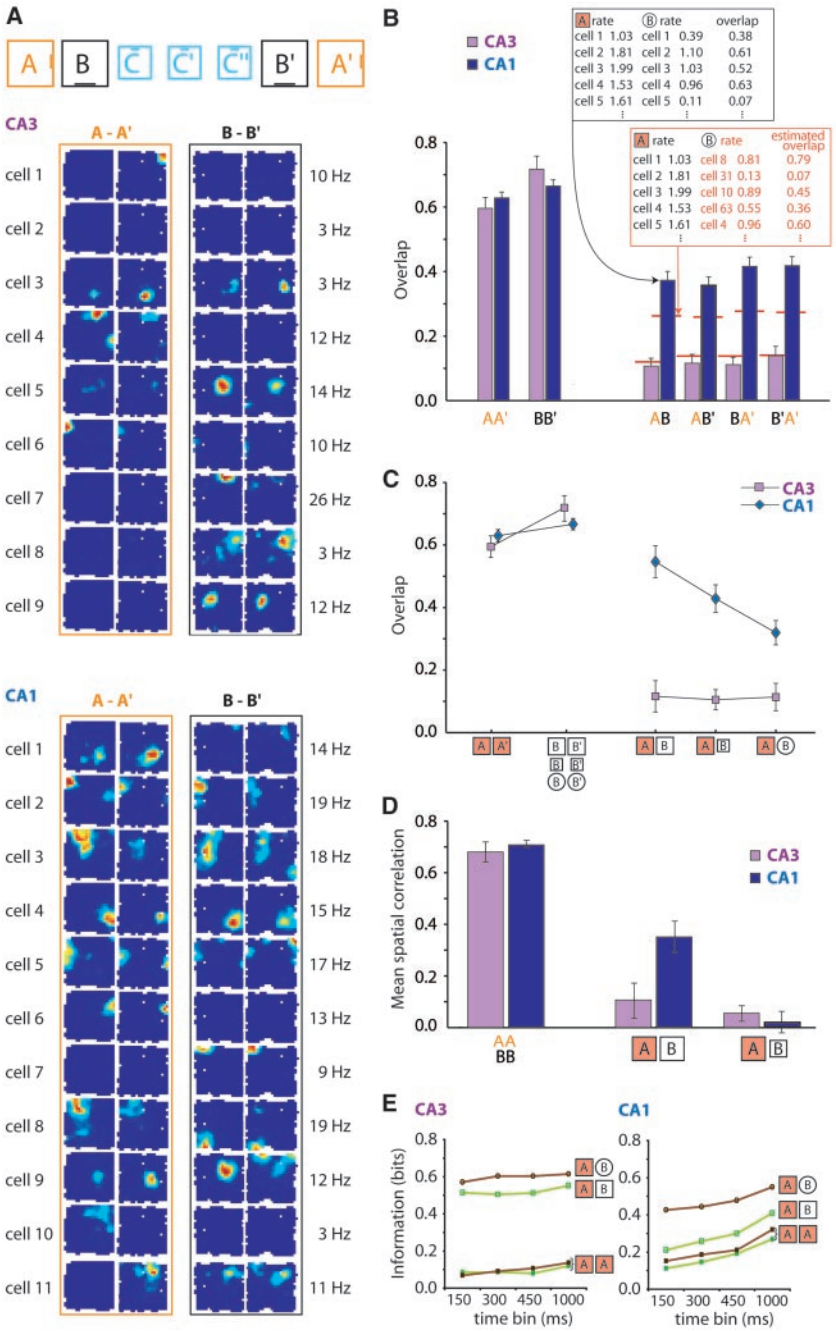

Fig. 2. Orthogonalized representations in CA3 but not CA1. (**A**) Color-coded rate maps showing place fields in identical enclosures but different rooms (day 10). Top section indicates recording sequence, geometry of test enclosures, and orientation of cue card (lines inside boxes). Spikes were recorded simultaneously from CA3 and CA1. Rows show cells; columns show trials in rooms A and B (not chronologically ordered). Plots are scaled to indicate maximum rates (red, maximum; blue, silent; white, not visited). (**B**) Overlap between active populations in rooms A and B (mean ± SEM). Overlap was measured by averaging across cells the ratio between the lower and higher rates in a pair of trials (top inset). Red lines indicate overlaps expected by assuming independent firing in the two trials (bottom inset). (**C**) Overlap as a function of geometric similarity of the enclosures in rooms A and B. (**D**) Mean spatial correlation (± SEM) of place fields in rooms A and B (squares only) (SOM Text). (**E**) Effect of geometric similarity on ensemble coactivity in CA1 but not CA3 in two rats with more than eight simultaneously recorded cells in each area (brown, low similarity session; green, high similarity session). High information corresponds to distinct distributions of population vectors in rooms A and B.

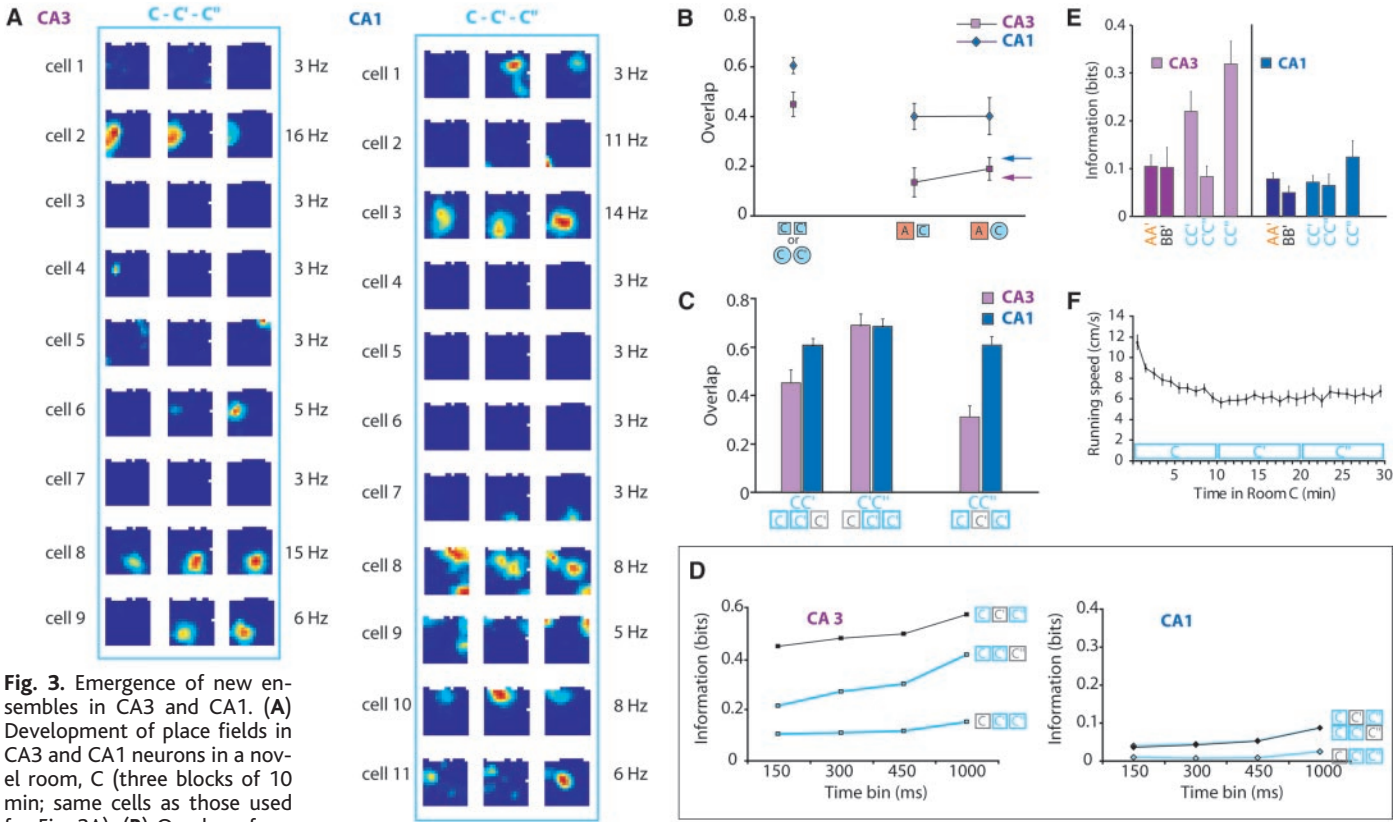

Fig. 3. Emergence of new ensembles in CA3 and CA1. (**A**) Development of place fields in CA3 and CA1 neurons in a novel room, C (three blocks of 10 min; same cells as those used for Fig. 2A). (**B**) Overlap of activity between rooms A (familiar) and C (novel). Enclosures had different sizes or both different sizes and different shapes. Arrows indicate expected values (purple, CA3; blue, CA1). (**C**) Overlap between pairs of 10-min blocks in room C (C, 0 to 10 min; C′, 10 to 20 min; C′′, 20 to 30 min). (D and E) Development of ensemble structure in CA3 and CA1 [(**D**) same experiment as in (A); (**E**) whole sample]. The difference in neuronal activity between early and late blocks of the trial was assessed by measuring how much information the distribution of population vectors provided about the part of the trial that was being recorded. (**F**) Horizontal speed during exploration of room C (mean ± SEM).

delayed changes of ensemble activity in this subfield (*34*, *35*). Whether these slower processes reflect the integration of inputs from CA3, conveying orthogonalized memory representations, with processed sensory information carried to CA1 by direct inputs from entorhinal cortex, remains to be determined.

Note added in proof: Additional evidence for CA1-CA3 differences is provided by a recent study measuring immediate early gene activation in two different novel rooms (*36*).

References and Notes

1. D. Marr, *Philos. Trans. R. Soc. Lond. Ser. B* **262**, 23 (1971).
2. J. O'Keefe, L. Nadel, *The Hippocampus as a Cognitive Map* (Clarendon, Oxford, UK, 1978).
3. L. R. Squire, *Psychol. Rev.* **99**, 195 (1992).
4. H. Eichenbaum, *Nat. Rev. Neurosci.* **1**, 41 (2000).
5. D. G. Amaral, M. P. Witter, *Neuroscience* **31**, 571 (1989).
6. A. Treves, *Hippocampus* **14**, 539 (2004).
7. R. U. Muller, J. L. Kubie, J. B. Ranck, *J. Neurosci.* **7**, 1935 (1987).
8. R. U. Muller, J. L. Kubie, *J. Neurosci.* **7**, 1951 (1987).
9. M. A. Wilson, B. L. McNaughton, *Science* **261**, 1055 (1993).
10. C. A. Barnes, B. L. McNaughton, S. J. Mizumori, B. W. Leonard, L. H. Lin, *Prog. Brain Res.* **83**, 287 (1990).
11. D. O. Hebb, *The Organization of Behavior* (Wiley, New York, 1949).
12. B. L. McNaughton, R. G. M. Morris, *Trends Neurosci.* **10**, 408 (1987).
13. A. Treves, E. T. Rolls, *Hippocampus* **2**, 189 (1992).
14. R. P. Kesner, P. E. Gilbert, G. V. Wallenstein, *Curr. Opin. Neurobiol.* **10**, 260 (2000).
15. G. J. Quirk, R. U. Muller, J. L. Kubie, J. B. Ranck Jr., *J. Neurosci.* **12**, 1945 (1992).
16. P. E. Sharp, *Behav. Brain Res.* **85**, 71 (1997).
17. W. E. Skaggs, B. L. McNaughton, *J. Neurosci.* **18**, 8455 (1998).
18. H. Tanila, *Hippocampus* **9**, 235 (1999).
19. L. E. Jarrard, *J. Comp. Physiol. Psychol.* **89**, 400 (1975).
20. Orthogonalization (pattern separation) refers to the tendency to decorrelate representations, assessed relative to the baseline expected for unrelated conditions. Orthogonalization is expressed as a difference in both the subset of active cells and the relative firing locations of cells that were active in each of the conditions (SOM Text). Remapping is a special case limited to the spatial domain.
21. A total of 146 CA3 and 244 CA1 pyramidal cells were compared across rooms in 10 rats. Sixty-four CA3 cells and 76 contralateral CA1 cells were recorded simultaneously (SOM Text).
22. V. H. Brun *et al.*, *Science* **296**, 2243 (2002).
23. G. Winocur, J. Olds, *J. Comp. Physiol. Psychol.* **92**, 312 (1978).
24. P. W. Frankland, V. Cestari, R. K. Filipkowski, R. J. McDonald, A. J. Silva, *Behav. Neurosci.* **112**, 863 (1998).
25. K. Nakazawa *et al.*, *Science* **297**, 211 (2002).
26. I. Lee, D. Yoganarasimha, G. Rao, J. J. Knierim, *Nature* **430**, 456 (2004).
27. A. Samsonovich, B. L. McNaughton, *J. Neurosci.* **17**, 5900 (1997).
28. R. Hirsh, *Behav. Biol.* **12**, 421 (1974).
29. S. G. Anagnostaras, G. D. Gale, M. S. Fanselow, *Hippocampus* **11**, 8 (2001).
30. M. L. Shapiro, H. Tanila, H. Eichenbaum, *Hippocampus* **7**, 624 (1997).
31. In retrospect, the stronger orthogonalization in CA3 provides an explanation for the divergent results obtained by two previous studies of place-cell remapping in visually identical environments (*17*, *18*). One of the procedural differences between these studies was the recording location. Remapping was complete when most cells were from CA3 (*18*) but only partial with recordings in CA1 (*17*).
32. J. H. Freeman Jr., C. Cuppernell, F. Flannery, M. Gabriel, *J. Neurosci.* **16**, 1538 (1996).
33. S. Leutgeb, S. J. Mizumori, *Neuroscience* **112**, 655 (2002).
34. C. Lever, T. Wills, F. Cacucci, N. Burgess, J. O'Keefe, *Nature* **416**, 90 (2002).
35. K. Nakazawa *et al.*, *Neuron* **38**, 305 (2003).
36. A. Vazdarjanova, J. F. Guzowski, *J. Neurosci.* **24**, 6489 (2004).

37. We thank I. M. F. Hammer, K. Haugen, K. Jenssen, S. Molden, R. Skjerpeng, and H. Waade for assistance and J. Knierim and O. Paulsen for comments. The work was supported by a Centre of Excellence grant from the Norwegian Research Council.

Supporting Online Material

www.sciencemag.org/cgi/content/full/1100265/DC1
Materials and Methods
SOM Text
Figs. S1 to S3
Tables S1 and S2
References and Notes

13 May 2004; accepted 8 July 2004
Published online 22 July 2004;
10.1126/science.1100265
Include this information when citing this paper.

Distinct Ensemble Codes in Hippocampal Areas CA3 and CA1

Stefan Leutgeb, Jill K. Leutgeb, Alessandro Treves, May-Britt Moser and Edvard I. Moser

Science **305** (5688), 1295-1298.
DOI: 10.1126/science.1100265originally published online July 22, 2004